Impulse Model Design of Acoustic Surface-Wave Filters

CLINTON S. HARTMANN, DELAMAR T. BELL, JR., AND RONALD C. ROSENFELD

Invited Paper

Abstract—**The design of surface acoustic wave bandpass filters which utilize interdigital electrode transducers is reviewed. The impulse-response description of interdigital transducers is extended to allow calculation of transducer input admittance and filter frequency response with much less effort than required by earlier equivalent-circuit model approaches. The application of the impulse model to the straightforward design of VHF and higher frequency bandpass filters is discussed and several examples of high-performance surface-wave bandpass filters are given.**

I. Introduction

THE ANALYSIS and design of interdigital surface-wave transducers by an impulse-response description has been discussed by several authors [1]–[3]. The impulse-response approach is a natural one because of the correspondence between the location of the interdigital fingers of the transducer and the signal generated by an impulse of acoustic energy traveling under the fingers. This paper extends the impulse-response model to include the calculation of transducer impedances and the effect of electrical loading on filter response. The model developed here provides comparable accuracy to the well-known equivalent-circuit approaches [2], [4] but with much less computation effort. This is due to the use of fast Fourier transforms (FFT) [5] instead of the detailed network analysis required by circuit models. The simplicity of the impulse model makes it very useful for the design of practical filters with prescribed responses.

Acoustic surface waves have many similarities with bulk acoustic waves which have been used for many years in resonator crystals, bandpass filters, delay lines, and dispersive filters [6]. They share the low wave velocity which results in compact devices and the low propagation loss which makes possible the very high Q's which can be achieved in acoustic filters.

Surface waves, however, are different in several ways which significantly enhance their usefulness. First, since a surface wave propagates at the surface, it is accessible along its entire propagation path as opposed to a bulk wave which is only accessible at the ends of the crystal. This allows for the simultaneous sampling of the waves at many points in the delay path and results in an important flexibility of surface-wave device functions which cannot be duplicated easily by bulk-wave filters. The second major advantage of surface-wave devices is the simplicity of the fabrication process for interdigital transducers. Basically, it consists of optically polishing the single surface of the piezoelectric substrate, evaporating or otherwise depositing a metal film, and then patterning the metal to form the transducers using standard photolithography techniques which have been highly developed for the semiconductor industry. This process is very inexpensive, highly repeatable, and, most important, it can be used to produce filters for the VHF and UHF ranges where other filter technologies have very limited capabilities. For example, many state-of-the-art semiconductor devices are using 1-μm electrode widths. An interdigital transducer with 1-μm electrodes corresponds to a surface-wave operating frequency of approximately 1 GHz (depending on the velocity of the substrate which is used). Another advantage of the surface-wave devices is that the substrate can be arbitrarily thick for mechanical strength, whereas the extremely small thickness of VHF bulk crystal filters makes them extremely fragile.

This paper considers analysis and design of interdigital surface-wave filters based on an impulse-response model. Section II considers the basic relations for an impulse-response description of a filter and the design of desirable impulse responses for good filter performance. The electrical input admittance is calculated in Section III based on extensions of the impulse-response description which leads to an analysis of electrical loading effects. Some of the more important design considerations, such as insertion loss, substrate choice, and weighting, are considered in Section IV. Section V provides a brief summary of an orderly procedure for making various design decisions, but a complete design procedure which considers all important distortion effects is beyond the scope of this paper. The paper concludes with several design examples which illustrate the wide variety of bandpass characteristics that can be achieved with surface-wave filters. Although the discussion in this paper is directed toward nondispersive filters, the theory and procedures given here apply with only minor changes to the design of dispersive, matched filters.

II. Impulse-Response Approach to Filter Analysis and Design

A. Relationship Between Transducer Geometry and Transducer Impulse Response

Fig. 1(a) shows a representative surface-wave filter consisting of a piezoelectric substrate on which are deposited two interdigital transducers, each consisting of interdigitated metal fingers connected to common bonding pads on either side of the acoustic beam. The input transducer T_1 generates a spatially periodic electric field with a periodicity determined by the spacing of the adjacent electrodes. This field generates surface waves through the piezoelectric effect with maximum efficiency at the frequency f_0 where the acoustic wavelength equals the periodicity L of the transducer. Other frequencies have reduced generation efficiency due to the cancellation of waves generated at one end of the transducer with those at the opposite end. The generated surface wave propagates to the output transducer T_2, which senses the electric fields which accompany the wave due to the piezoelectric effect. Again the degree of match between the surface-wave wavelength

Manuscript received September 25, 1972; revised December 11, 1972.
The authors are with Texas Instruments Incorporated, Dallas, Tex. 75222.

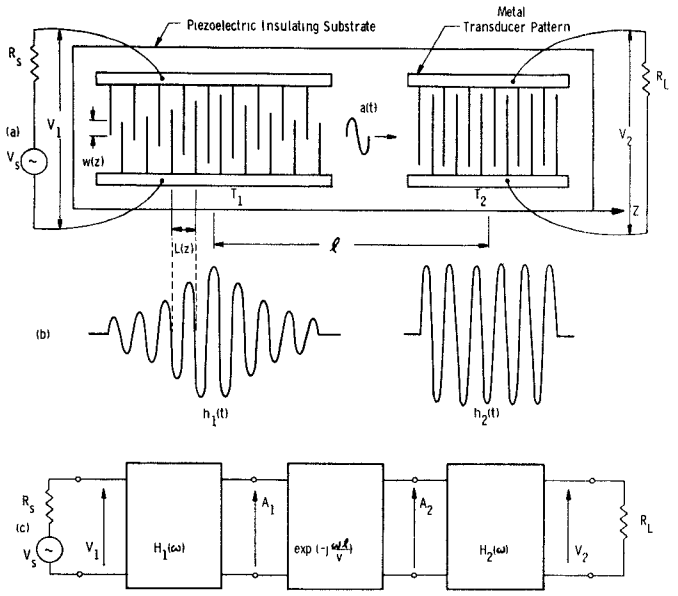

Fig. 1. Surface-wave bandpass filter. (a) Representative device geometry. (b) Effective impulse response. (c) Representation for linear filter theory.

and the transducer period determines the relative conversion efficiency.

The filtering properties of these devices are completely determined by the processes for conversion of the electrical signal to acoustic energy, and vice versa, at the input and output transducers. This is shown in Fig. 1(c) which schematically describes the device as two frequency selective transfer functions, $H_1(\omega)$ and $H_2(\omega)$, connected by a broad-band time delay $\exp(-j\omega l/v)$. Here l is the distance between the centers of the two transducers as shown in Fig. 1(a) and v is the surface-wave propagation velocity. The total transfer function of the device is then approximately given by

$$\frac{V_2}{V_1} \simeq H_1(\omega)\ \exp(-j\omega l/v) \cdot H_2(\omega). \tag{1}$$

The transducer transfer functions $H_i(\omega)$ can be calculated from the transducer impulse responses (i.e., the generated acoustic waveform which occurs when a voltage impulse is applied across the electrical input terminals). This impulse response $h(t)$ is a waveform which has a particularly simple relationship to the transducer geometry since each electrode pair constitutes a tap on the acoustic delay line whose relative time delay is given by the position of the electrode pair on the surface-wave substrate, and whose strength is directly proportional to the amount of overlap $W(z)$ between adjacent electrodes. For example, Fig. 1(b) shows the effective impulse responses of the two transducers in Fig. 1(a), and, as can be seen, each half cycle in $h(t)$ corresponds to a particular gap between adjacent electrodes of opposite polarity.

From filter theory it is known that the impulse response $h(t)$, and the frequency response $H(\omega)$, are a Fourier transform pair [7], and thus the frequency response can be calculated by means of a Fourier transform:

$$H(\omega) = \int_{-\infty}^{\infty} h(t)\ \exp(-j\omega t)\ dt. \tag{2}$$

Conceptually, any desired frequency response can thus be

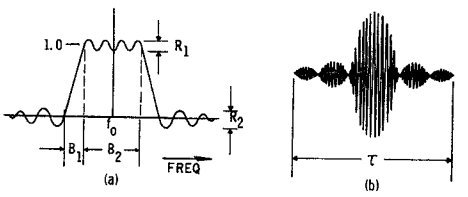

Fig. 2. Specification of filter response (a) Frequency response with transition bandwidth B_1, ripple R_1, sidelobe level R_2, and pass bandwidth B_2. (b) Corresponding impulse response with finite length τ.

obtained by simply taking the inverse Fourier transform of this desired frequency response and placing electrodes on the substrate surface corresponding to the calculated impulse response

$$h(t) = \frac{1}{2\pi}\int_{-\infty}^{\infty} H(\omega)\ \exp(j\omega t)\ d\omega. \tag{3}$$

There are, however, two fundamental restrictions on the type of frequency responses which can be obtained. First, only bandpass functions can be realized. Second, the impulse responses of the surface-wave devices must be of a finite length due to the finite length of the available surface-wave substrates. This second restriction has a corresponding frequency-response limitation on filter-skirt steepness and on maximum filter time delay.

B. Filter Design by Designing an Impulse Response

Since the impulse response of a transducer is directly related to electrode placement and length, a desired filter function can be obtained by designing a device with any impulse response whose Fourier transform has the desired frequency response. Specification of an appropriate transducer impulse response is relatively simple for pulse compression filters and phase-shift keyed (PSK) matched filters since the specification of these filters is usually given in impulse-response form. However, if specifications are given in the frequency domain, a waveform design problem exists.

Fig. 2 shows a typical bandpass filter response which is characterized by five parameters: 1) the center frequency f_0, 2) the transition bandwidth B_1, 3) the pass bandwidth B_2, 4) the ripple level R_1, and 5) the sidelobe level R_2. Sometimes the skirt selectivity is specified by a shape factor S, which is equal to the ratio of the bandwidth at the rejection level to the pass bandwidth

$$S = (2B_1 + B_2)/B_2. \tag{4}$$

The impulse response required to produce this frequency response is shown schematically in Fig. 2(b) with a time length τ. The optimum design will result in a minimum length τ, which allows one to obtain the desired transition bandwidth, pass bandwidth, ripple, and sidelobe level. For most designs the transition bandwidth and the sidelobe level are the dominant factors in determining this minimum τ, although an extremely low ripple level can extend this length somewhat.

Considerable work on finding good and sometimes the best possible impulse response has been performed in designing nonrecursive digital filters [8]. A near approach to the optimum waveform for maximum skirt steepness and maximum sidelobe rejection can be obtained by using a Dolph–Chebyshev window function [9] on the idealized rectangular fre-

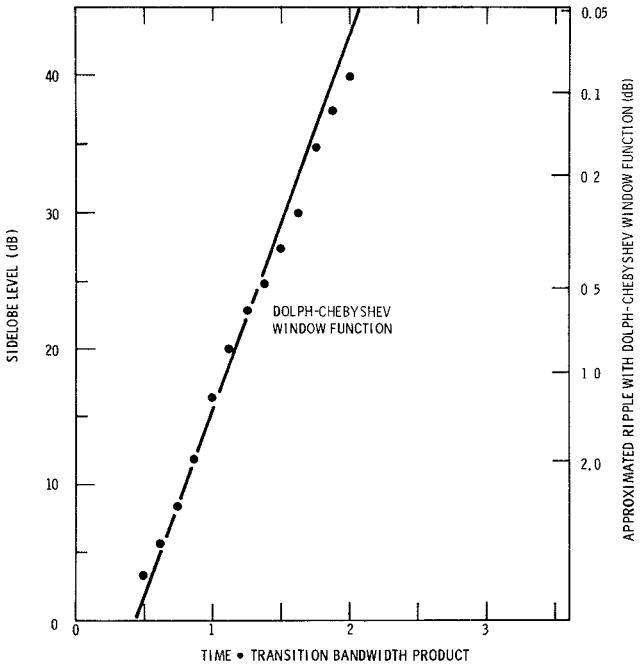

Fig. 3. Maximum sidelobe rejection as a function of impulse-response length-transition bandwidth product. Solid line: Approximate result using Dolph–Chebyshev window function. Solid points: Impulse response derived using iterative optimization.

quency response of an ideal bandpass filter (see Appendix I). From these functions, one finds that the minimum impulse-response length for satisfying a given specification is approximately given by

$$\tau_{\min} \simeq (0.73/B_1) \log R_2. \tag{5}$$

This relationship is plotted in Fig. 3 showing maximum achievable sidelobe rejection as a function of the impulse-response time length multiplied by the transition bandwidth. The points on the curve correspond to various designs done by use of an iterative optimizing scheme. As can be seen, one can slightly improve on the Dolph–Chebyshev window function with the iterative optimizing scheme, but the window-function technique provides an excellent approximation to the ideal. The ordinate on the right-hand side of the figure shows the approximate ripple level which would be associated with different sidelobe levels using the Dolph–Chebyshev window functions. These are only approximate and are most nearly correct for very low shape-factor cases. For filters with more moderate shaped factors (i.e., 2:1 or larger) one finds that considerably less ripple can be obtained than would be indicated by these numbers.

An example of what can be gained in device performance through optimization is illustrated by Fig. 4 which shows frequency responses corresponding to a truncated sin x/x weighting function and an optimized impulse response of the same length for the same bandwidth. As can be seen, the optimization reduced the peak sidelobe level by approximately 6 dB, but more important it reduced the bandpass ripple from 2 dB to less than 0.1 dB. This ripple reduction is extremely important because normally two such responses would be cascaded to obtain the overall filter response. The only degradation in the optimized function is that the far-out

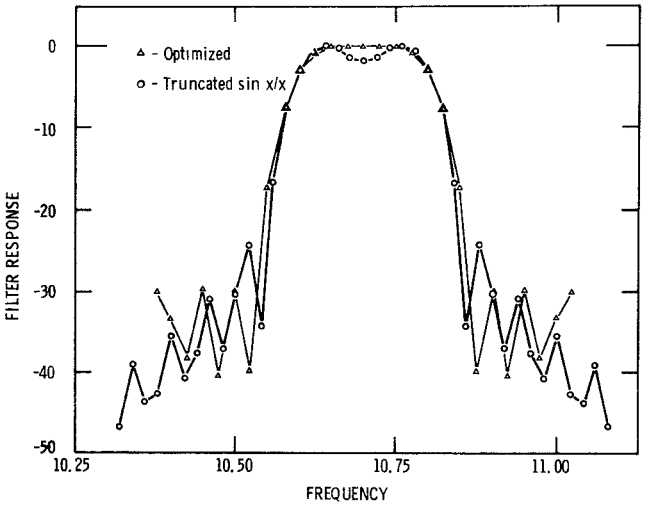

Fig. 4. Comparison of frequency responses corresponding to a truncated sin x/x (one sidelobe) and an optimized impulse response of the same length.

sidelobes have been raised in amplitude to more nearly correspond to the amplitude of the near-in sidelobes. This is the slight penalty which is paid for improved filter performance.

III. An Impulse-Response Model for Calculating Transducer Input Admittance and Electrical Loading Effects

The impulse-response description of surface-wave device operation as presented in the preceding section is a special case in which it was assumed that the electrical source admittance was very large compared to the transducer input admittance. In most practical devices this assumption is not justified because these admittances are usually designed to be approximately equal to minimize insertion loss. The resulting electrical loading effect is calculated in this section by extending the impulse-response description given earlier to include the calculation of an interdigital transducer's input admittance. This section will only concern analysis of the effect; the design implications are considered later in Section IV.

A. Impulse Response of an Interdigital Transducer

Calculation of a transducer's input admittance requires that its impulse response be specified more accurately than the simple description given in Fig. 1(b). The surface-wave amplitude is given below in terms of a variable $a(t)$ whose square is the power flow in the acoustic beam. This definition is chosen for simplicity because later development of the model depends on conservation of energy arguments. If an observable quantity such as stress, strain, or particle velocity had been chosen then unnecessary complication would be added to the model due to the frequency-dependent penetration depth of the surface wave. The relationship between $a(t)$ and a directly observable quantity can be obtained by solving for the acoustic power in the beam in terms of that quantity and simply taking a square root. The particular surface-wave amplitude which occurs when the transducer is electrically driven by a voltage impulse will be denoted by $h(t)$ to differentiate it from the surface-wave amplitude $a(t)$ which occurs under arbitrary excitation.

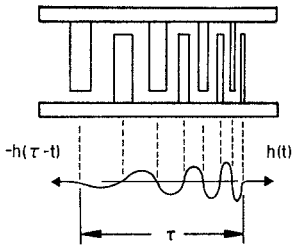

Fig. 5. Construction of the impulse response of a uniform overlap array with variable electrode center-to-center spacing.

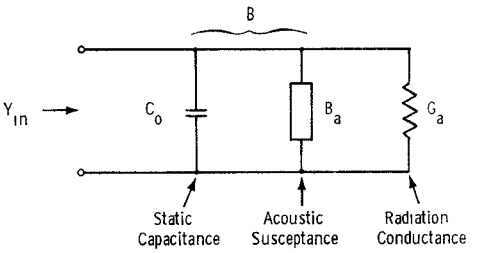

Fig. 6. Electrical equivalent input admittance of a surface-wave transducer.

In constructing the impulse response of an interdigital transducer, various authors have used sine waves [10], impulses [2], and rectangles [3] to describe the shape of the waveform generated by a single electrode pair in the transducer. All of these assumptions give very similar results near the fundamental frequency of the transducer, but none give the correct harmonic response. A more accurate waveshape may be obtained by using a waveform which is related to the electrostatic field between the electrodes [11]. Since only the fundamental frequency component of an interdigital transducer's response is considered here, sine waves will be used because this waveshape simplifies the mathematics associated with the model.

Fig. 5 illustrates a useful method for constructing the impulse response $h(t)$ of a uniform overlap transducer array with variable center-to-center spacing of the electrodes but constant electrode width-to-gap ratio. The results will be generalized later for arrays with nonuniform overlap, and if variable finger width-to-gap ratio is encountered, proper compensation must be made as described by Engan [11]. First, place one-half cycle of a sine wave in $h(t)$ for each interaction between electrodes of opposite polarity, with the time spacing of the zero crossings equal to the surface-wave propagation delay between the electrode centers. (The phase of $h(t)$ is arbitrarily chosen with zero crossings on the electrodes for simplicity. Other equally valid choices are possible if desired.) Second, the amplitude of each half cycle is multiplied by $f_i^{3/2}$, where f_i is the instantaneous frequency at that point in the array. (The instantaneous frequency is simply that frequency with a period of a half cycle equal to the period of the half cycle used here.) The origin of this frequency dependance is given in Appendix II. Third, multiply the overall response by $K\sqrt{W}$, where K is a measure of the surface-wave coupling efficiency which is characteristic of the substrate under consideration and W is the acoustic beamwidth. The dependence on $\sqrt{W}$ is necessary since the impulse response is the square root of the acoustic power in the beam.

Calculation of the coupling efficiency K is outside the scope of this model and must be determined by other means. To first order, K may be evaluated by solving the impulse model for an N finger-pair transducer (given below as an example) and equating the results to the results of an identical example solved by means of the equivalent-circuit model [4]. By this technique, it can be shown that

$$K\sqrt{W} = 4k\sqrt{C_s} \tag{6}$$

where k is the familiar coupling coefficient for surface waves and C_s is the capacitance per finger pair (which varies linearly with the acoustic beamwidth W). Values of C_s and k for several substrates of interest are given later in Table I.

To summarize the previous discussion, the impulse response is given by

$$h(t) = 4k\sqrt{C_s}f_i^{3/2}(t)\sin\theta(t) \tag{7}$$

where

$$\theta(t) = 2\pi\int_0^t f_i(\tau)\,d\tau \tag{8}$$

t is the impulse-response time coordinate given by $t=z/v$, and v is the acoustic wave velocity.

B. Input Admittance of a Surface-Wave Transducer

The input admittance of a surface-wave transducer can now be obtained by calculating the energy in the impulse response as constructed above and then assuming that all the electrical energy dissipation at the transducer input is accounted for by acoustic radiation. Let $H(\omega)$ denote the Fourier transform of the transducer impulse response $h(t)$ as determined earlier in (7). In the frequency domain, the sum of the energy per unit frequency radiated from both sides of an interdigital transducer when driven by a unit impulse is given by

$$\begin{aligned} E(\omega) &= H(\omega)\cdot H^*(\omega) + H^*(\omega)\exp(-j\omega\tau)\cdot H(\omega)\exp(j\omega\tau) \\ &= 2\,|\,H(\omega)\,|^2 \end{aligned} \tag{9}$$

where $-H^*(\omega)\exp(-j\omega\tau)$ is the Fourier transform of the impulse response of the transducer in the reverse direction, and τ is the impulse-response time duration of the transducer shown in Fig. 5.

This same energy manifests itself as dissipation in the acoustic radiation conductance $G_a(\omega)$ as shown in Fig. 6. The energy per unit frequency delivered to $G_a(\omega)$ is given by

$$E(\omega) = V_{\text{in}}^2(\omega)G_a(\omega). \tag{10}$$

For the unit impulse excitation considered above $V_{\text{in}}(\omega)=1$; thus,

$$E(\omega) = G_a(\omega). \tag{11}$$

By equating (9) and (11), one obtains for the real part of the input admittance

$$G_a(\omega) = 2\,|\,H(\omega)\,|^2. \tag{12}$$

Thus the real part of the input admittance of a surface-wave transducer is equal to twice the squared magnitude of the Fourier transform of the impulse response.

Since this transducer is a causal system, it follows that the imaginary part of the input admittance is the Hilbert transform of the real part as was recently pointed out by Nalamwar and Epstein [12]

$$B_a(\omega) = \frac{1}{\pi}\int_{-\infty}^{+\infty} \frac{G_a(\omega')}{\omega' - \omega}\, d\omega'. \tag{13}$$

This relationship is ambiguous to the extent that there can be an additional additive capacitance, inductance, or constant susceptance which would not be described by the transform. For this case, the Hilbert transform of G_a can be identified as the radiation susceptance, while an additional term is required to account for the susceptance of the static capacitance of the interdigital array. The static capacitance is found by multiplying the number of electrode interaction pairs by C_s, the capacitance per pair:

$$C_0 = NC_s. \tag{14}$$

Values of C_s are given later in Table I. Thus all the elements of the electrical input admittance shown in Fig. 6 have been calculated.

C. Input Admittance of an N-Pair Transducer

The input admittance of an N-interaction-pair transducer will be calculated here as an example of the use of this model. The impulse response of such a transducer can be calculated by means of (7):

$$\begin{aligned} h(t) &= f_0^{3/2} 4k\sqrt{C_s} \sin \omega_0 t, \qquad 0 \le t \le \frac{N}{f_0} \\ &= 0, \qquad\qquad t < 0, \frac{N}{f_0} < t. \end{aligned} \tag{15}$$

The corresponding Fourier transform is approximately given by

$$H(\omega) \cong 2k\sqrt{C_s f_0} N \frac{\sin X}{X} \exp\left(-j\omega N/2f_0\right) \tag{16}$$

where $X = N\pi(\omega - \omega_0)/\omega_0$. The real part of the radiation admittance can be obtained by using (12):

$$G_a(\omega) = 8k^2 C_s f_0 N^2 \frac{\sin^2 X}{X^2} = G_0 \frac{\sin^2 X}{X^2}. \tag{17}$$

The radiation susceptance (13), is given by the Hilbert transform of (17) which can be shown to be [13]

$$B_a(\omega) = \frac{G_0(\sin 2X - 2X)}{2X^2} \tag{18}$$

and the static capacitance is given by (14). These results are identical to ones obtained by Smith *et al.* [4], for the crossed-field equivalent-circuit model, except that much less effort was necessary here to obtain these results. It should be pointed out that this impulse-response model cannot easily include either electrode edge reflection effects or model the differences which occur when an "inline" equivalent-circuit model is used. Both of these effects can be accounted for by suitable modification [14] of the equivalent-circuit model.

D. Modeling Arrays with Nonuniform Electrode Overlap

All the results up to this point have considered only transducers with uniform overlap, but nonuniform overlap arrays are a very important class of interdigital transducers because varying the finger overlap is probably the easiest, most reproducible method for controlling the amplitude of each individual half cycle in the impulse response of a transducer.

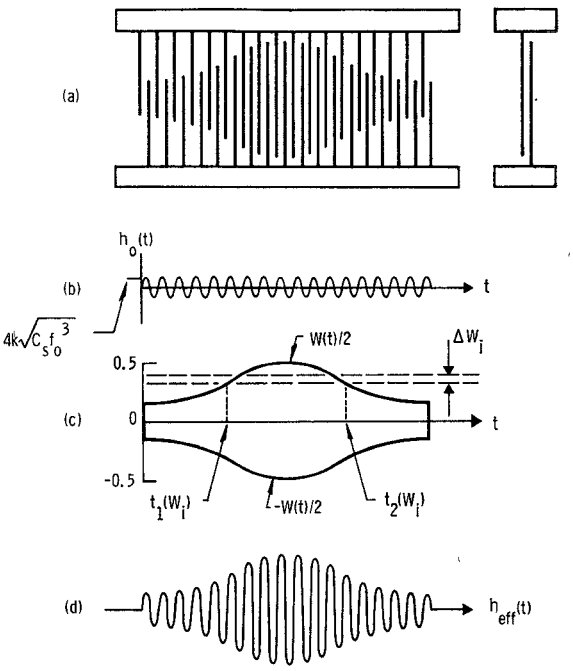

Fig. 7. Modeling of overlap weighted transducer. (a) Transducer schematic with second uniform overlap array. (b) Impulse response of transducer without overlap weighting. (c) Envelope of weighting function. (d) Effective impulse response.

The technique to be used here for modeling these arrays is similar to one described by Tancrell and Holland [2] for modeling overlap weighted arrays using the equivalent-circuit model. Fig. 7 illustrates this technique whereby the transducer is divided into narrow strips which have uniform overlap. Part (a) of the figure shows the overlap weighted transducer to be modeled, and parts (b) and (c) show two separate functions describing this array. The first function $h_0(t)$ describes the impulse response of a uniform overlap transducer with unit width and with the same finger placement as the transducer to be modeled. The second function describes the envelope of the overlap, denoted by $W(t)$. The two functions $t_1(W_i)$ and $t_2(W_i)$ describe the beginning and end points of the ith strip. The input admittance is then simply calculated by summing the admittances of all the various strips as the strips are all electrically in parallel.

$$G_a(\omega) = \sum_i 2\left|\int_{t_1(W_i)}^{t_2(W_i)} h_0(t) \exp\left(-j\omega t\right) dt\right|^2 \Delta W_i \tag{19}$$

where ΔW_i is the width of the ith strip and the term inside the magnitude symbol is simply the Fourier transform of the impulse response of a particular strip. The acoustic reactance is still given by (13) and the static capacitance can be calculated by summing the contributions from each strip.

The acoustic radiation from an overlap weighted transducer cannot be represented by a single acoustic port with a single impulse response. Instead there must be one port for each strip. However, as shown in [2], the acoustic transduction properties of this transducer can be represented by a single effective impulse response $h_{eff}(t)$ for the case where the second transducer in the device has a uniform overlap of a width equal to or greater than the largest overlap in the over-

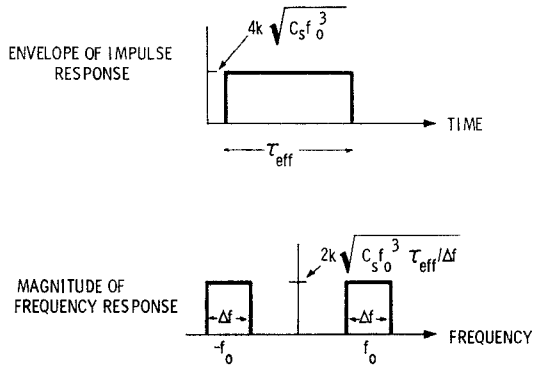

Fig. 8. Rectangular approximation for envelopes of the impulse and frequency responses of a surface-wave transducer.

lap weighted array. As illustrated in Fig. 7(d), $h_{eff}(t)$ is equal to the product of the two functions $h_0(t)$ and $W(t)$ defined in the preceding paragraph:

$$h_{eff}(t) = W(t)h_0(t)/\sqrt{W_{max}} \tag{20}$$

where W_{max} is maximum value of $W(t)$.

This result is due to the integrating effect of the second array over the acoustic beam of the first transducer. Note that this effective impulse response cannot be used for obtaining the device input admittance, nor will it provide proper results for the device transfer function if both arrays in a device are overlap weighted. To properly treat these items a full analysis of the device must be made using strips and possible acoustic beam-spreading effects should be considered as well.

E. Input Admittance of Dispersive Transducers

Dispersive filters are an important class of uses for surface-wave devices. For example, linear FM pulse-compression filters for radar [15], [16] and phase-coded matched filter pairs [17]–[19] for spread spectrum communications are common applications. Many of these filters are normally characterized by an effective time length τ_{eff} of the impulse response and a bandwidth Δf of the frequency response as shown in Fig. 8. Only the envelope of the impulse response is shown and only the magnitude of the frequency response is shown. Reasonably good rectangular approximations can be made to a large number of different transducer time and frequency responses which are of interest. From a knowledge of the transducer center frequency, beamwidth, and substrate type, the amplitude of the impulse response is known to be $4k\sqrt{C_s}f_0^{3/2}$ as given by (7). Parsavall's theorem [13] states that the energy in the time- and frequency-domain representations of a function must be equal:

$$\int_{-\infty}^{\infty} |h(t)|^2\,dt = \int_{-\infty}^{\infty} |H(2\pi f)|^2\,df. \tag{21}$$

Since $h(t)$ is a pure real sinusoidal type of waveform, the integral of $|h(t)|^2$ is half of the peak value squared times the time length τ_{eff}

$$\int_{-\infty}^{\infty} |h(t)|^2\,dt = \frac{(4k\sqrt{C_s}f_0^{3/2})^2\tau_{eff}}{2}. \tag{22}$$

The function $H(2\pi f)$ is complex with an assumed uniform amplitude and thus the factor of $\frac{1}{2}$ does not occur in this integral, but account must be made for both the positive and negative frequency components. Thus

$$\int_{-\infty}^{\infty} |H(2\pi f)|^2\,df = |H(2\pi f_0)|^2 2\Delta f. \tag{23}$$

Now by using (21)–(23), one obtains

$$|H(\omega_0)|^2 = \frac{4k^2C_sf_0^3\tau_{eff}}{\Delta f}. \tag{24}$$

Knowledge of the magnitude of the Fourier-transformed impulse response is sufficient to calculate the real part of the input admittance as shown by (12):

$$G_a(\omega_0) = \frac{8f_0^3k^2C_s\tau_{eff}}{\Delta f}. \tag{25}$$

Two alternative forms for this relationship have proven useful. First, by setting $\tau_{eff}f_0 = N_{tot}$, the effective total number of electrode interaction pairs in the array, one obtains

$$G_a(\omega_0) = \frac{8f_0k^2C_sN_{tot}^2}{\tau_{eff}\Delta f}. \tag{26}$$

The numerator is simply the peak radiation conduction which occurs if all the electrodes were resonant at the device center frequency [see (17)]. Thus one simply uses this value and divides by the time–bandwidth product.

The second form for writing (25) is

$$G_a(\omega_0) = 8f_0k^2C_s\left(\frac{f_0}{\Delta f}\right)^2\tau_{eff}\Delta f. \tag{27}$$

The quantity $(f_0/\Delta f)$ is equal to the number of electrodes required in a linear nondispersive transducer to obtain this particular fractional bandwidth. Thus this form of the equation says that one calculates the input admittance of nondispersive transducer with the same bandwidth, center frequency, and beamwidth as the dispersive filter in question, and then multiplies the result by the time–bandwidth product of the device.

The input susceptance again consists of an acoustic radiation susceptance and a static capacitance. The acoustic susceptance will be ignored here because it is zero at the center frequency and usually much smaller than the static capacitance contribution at other frequencies. Its shape depends critically on the shape of the $G_a(\omega)$ which is only approximately correct in the rectangular approximation used here. Thus,

$$B(\omega) \simeq 2\pi f N_{tot}C_s. \tag{28}$$

By taking the ratio of (26) and (28) and appropriately rearranging the terms, one obtains the electrical radiation Q of the device.

$$Q_r = B/G_a = \frac{\pi}{4k^2}\frac{\Delta f}{f_0}. \tag{29}$$

This result is extremely useful because it says that the radiation Q depends on only the fractional bandwidth of the transducer and on the coupling coefficient of the substrate. Hence, if one knows the input admittance on a particular substrate for a particular fractional bandwidth device, one can simply scale the results by the time–bandwidth product to obtain the input admittance of the corresponding pulse compression

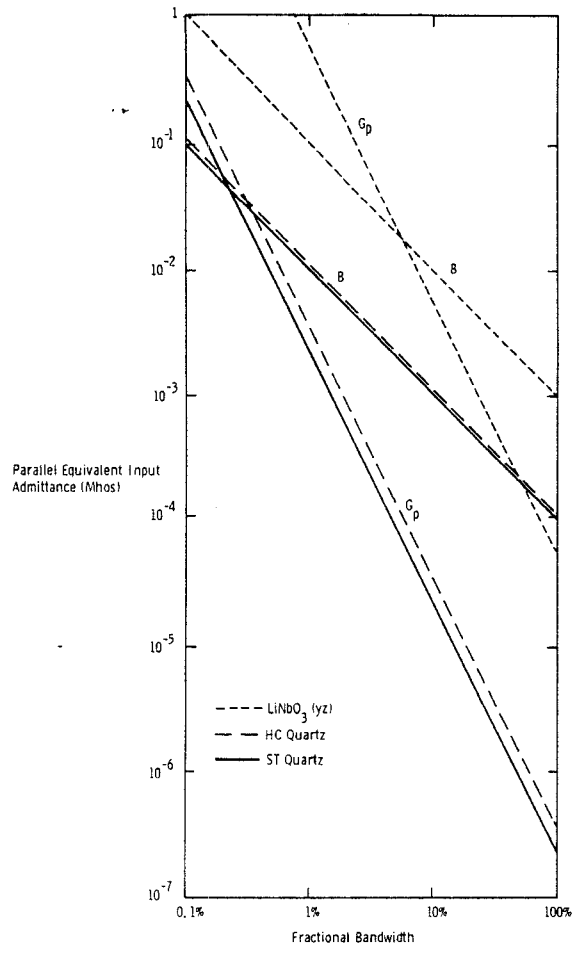

Fig. 9. Approximate input admittance of surface-wave transducer with 100-λ beamwidth. Scale both B and G if different beamwidth is used. Multiply B and G by time–bandwidth product for dispersive transducers.

transducer with the same bandwidth. Thus one can draw universal input admittance curves as shown in Fig. 9. Admittance is plotted on the vertical axis and fractional bandwidth is plotted horizontally. The curves shown are for a beamwidth of 100 wavelengths and for two different substrate materials which are commonly used, quartz and lithium niobate. If nondispersive transducers are being considered, one simply reads the appropriate values and scales the numbers for the actual device beamwidth. In addition, if the transducers are dispersive then one simply multiplies the numbers as well by the time–bandwidth product of the transducer.

In general, the rectangular approximation used above works best for large time–bandwidth products (>100). However, since an N period single-frequency transducer has a time–bandwidth product of unity, the above equation has a correct limiting form even for the small time–bandwidth products ($\tau\Delta f < 1$ is physically meaningless). Since the rectangular approximation can never be exactly satisfied in both the time and frequency domain, the above results are never obtained exactly; however, it does provide an excellent approximation which can be used in a variety of cases. If more accuracy is desired for a particular device, some other method, such as is described in Section III-B, must be used to calculate the impedance.

For cases which do not satisfy the rectangular approximation, but for which the shape of the impulse response and the

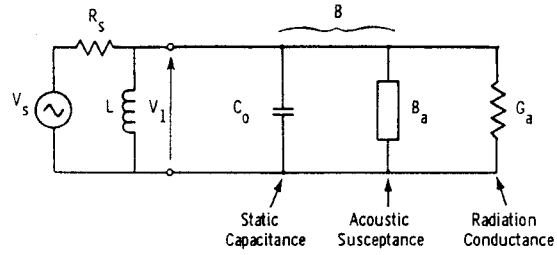

Fig. 10. Electrical equivalent circuit for matched surface-wave transducer.

frequency response are known, the conservation of energy principle can still be used to evaluate the amplitude of the spectrum, and hence the magnitude of the radiation conductance. An example of this occurs in phase-coded arrays wherein the coded transducer consists of numerous widely spaced taps consisting of a few fingers each with appropriate phase reversals to effect the coding. (See for example [14, fig. 16(a)].) The impulse response consists of a train of RF bursts while the bandwidth of the transducer is equal to the bandwidth of a single tap. In this case, the above relationships can still be used, since the energy will be correctly given if τ_{eff} is taken to be the sum of the impulse-response lengths of the individual RF bursts and the bandwidth is set equal to the bandwidth of a single tap.

F. Computation Techniques

Use of the impulse-response model can be easily implemented by using an FFT [5] computer routine to provide a sampled Fourier transform of the impulse response of the filter. This can then be used to calculate $G_a(\omega)$. A Hilbert transform can be effected by using an inverse FFT, multiplication by j signum (x) $(= -j$ for $x<0$ and $+j$ for $x>0)$, and using a second FFT [13]. In this manner, the acoustic susceptance is also obtained over the entire frequency range. This impulse-response model [20] has recently been extended by Mitchell and Reilly [21] to provide a complete Y-matrix description of a surface-wave device in terms of the admittances calculated above. Due to the computation efficiency of the FFT routine, this is an effective method for obtaining a complete description of a surface-wave filter over the entire frequency range from dc to the second harmonic.

The impulse response is much easier to use than the equivalent-circuit model and it provides identical results with the crossed-field [4] version of this model when electrode reflection effects are ignored [14]. For this reason, no detailed numerical examples have been given here because various authors [1], [2], [4] have presented such data.

G. Electrical Loading Effects

The transfer function of a surface-wave transducer has been calculated above for the special case where the voltage on the transducer terminals is equal to the source voltage. This is equivalent to assuming that the source has zero impedance. In practice, however, the source has finite impedance and, since the transducer has finite input admittance, the voltage at the transducer terminals can differ significantly from the source voltage. The effects of this electrical loading can be calculated by solving for the actual voltage which appears on the transducer terminals and multiplying this voltage by the above transfer function which is calculated from the impulse response.

The method will be illustrated by including the effects of a matching inductance L and finite source impedance $R_s = 1/G_s$, as shown in Fig. 10. The transfer function from the electrical source to the generated acoustic wave can be evaluated by solving for the voltage $V_1(\omega)$ across the transducer and multiplying by the Fourier transform of the impulse response $H_1(\omega)$ constructed earlier in Section III-B. With reference to Fig. 1(c)

$$\frac{A_1(\omega)}{V_s} = \frac{V_1(\omega)}{V_s} \cdot H_1(\omega) = \frac{G_s H_1(\omega)}{G_s + \dfrac{1}{j\omega L} + j\omega C_0 + jB_a(\omega) + G_a(\omega)} \cdot \quad (30)$$

This equation shows that the frequency dependence of the acoustic input admittance causes three characteristic effects. First, the electrical response of the matching inductor L with the device static capacitance causes a rounding of the filter bandpass and a phase response modification which is characteristic of a single damped pole. Second, the acoustic reactance $B_a(\omega)$ is zero at the device center frequency, but it demonstrates a positive and a negative swing with an amplitude of the same order as $G_a(\omega)$. This causes both amplitude and phase ripple, but the latter is usually the most noticeable. Typical values vary from $\pm 1°$ to $\pm 10°$ depending on how well the filter is matched electrically. The third effect is the degradation of sidelobe rejection as a device is matched. In (30), the transfer function follows $H_1(\omega)$ as long as G_s is the dominant term in the denominator. However, if the device is well matched, then G_s equals $G_a(\omega_0)$ at the center frequency, but the frequency dependence of $G_a(\omega)$ is such that it is much smaller than G_s at the sidelobe frequencies. By examination of (30), it is observed that if the matching Q is sufficiently low, such that the reactive terms in this equation are negligible, then the transfer function at the sidelobe will be twice as large as is predicted by $H_1(\omega)$ alone. This corresponds to a 6-dB sidelobe degradation. Since two transducers are used, the potential degradation of sidelobe rejection is 12 dB. The full 12-dB effect is normally not observed in practice because the matching networks are still partly effective at the close sidelobes and the far sidelobes are low enough to not matter. A 10-dB design margin is usually adequate for most filter designs.

IV. Important Design Considerations

Before considering the application of the impulse model to the design of surface-wave filters in Section V, several other aspects of device design and operation must be considered to place the design procedure in proper context. The items covered in this section include 1) division of a desired filter response into two responses to be realized by two separate transducers, 2) distortion effects, 3) sources of insertion loss, and 4) choosing a substrate.

A. Weighting Configuration

Designing a surface-wave filter requires the division of the overall frequency response into two responses to be realized by two separate transducers. Probably the simplest such division was illustrated in Fig. 7(a), where one transducer was apodized [2] in accordance with a desired impulse response and the second transducer was a broad-band array with only a few finger pairs. The advantages of this configuration are that only a single transducer needs to be designed, and that the overlap weighting technique is easy to implement and works well when the second transducer is of uniform beamwidth. The potential disadvantages of this configuration are: 1) the total burden for producing a given response falls on one transducer; 2) the wide bandwidth of the second array can cause additional insertion loss (see Section IV-C); and 3) the unweighted second array can cause undesired rounding of the filter response due to its sin $(X)/X$ frequency response.

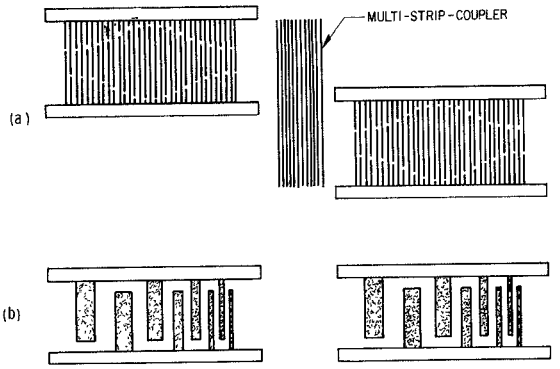

Fig. 11. Configurations for weighting surface-wave filters. (a) Multistrip coupler allows use of two overlap weighted arrays in a single filter. (b) Two phase-weighted transducers with opposite dispersion for canceling phase nonlinearity.

A seemingly obvious improvement is to use two overlap weighted transducers because all the difficulties are associated with the unweighted second array. Unfortunately, this causes more problems than it solves for several reasons. First, the one-to-one correspondance between the effective impulse response of an overlap weighted array given by (20) and the length and position of the electrodes in the array only applies if the electrodes in the second array have a uniform overlap. If both arrays are overlap weighted, then a unique impulse response cannot be assigned to either array, and the two cannot be designed independently. Tancrell [2] and Smith [22] have published analyses of the configuration with two overlap weighted arrays, both of which assumed that beam-spreading effects were negligible. Smith's slightly more approximate analysis allowed him to devise a synthesis technique which can be used only for designing FM pulse-compression filters using two overlap weighted arrays. However, the benefit of having both arrays weighted is somewhat illusory because the amount of weighting (ratio of the maximum overlap to the minimum overlap) required of each array is equal to the amount of weighting which would have been required on the one weighted array if the weighted–unweighted configuration of Fig. 7(a) had been used. The authors have designed nondispersive filters using Tancrell's analysis and found a result similar to Smith's. The resulting experimental devices were severely degraded due to the effects of beam spreading.

A technique whereby two overlap weighted transducers can be used and designed in terms of independent impulse responses is to couple the two transducers through a multistrip coupler [23], as shown in Fig. 11(a). In this case, the coupler performs the necessary integration across the beamwidth such that a unique impulse response can be assigned to each transducer. Unfortunately, the multistrip coupler is only practical on high coupling substrates such as lithium niobate.

A phase-weighting technique for obtaining a specified frequency response is illustrated in Fig. 11(b). The technique requires the synthesis of a uniform amplitude waveform with

appropriate phase modulation for obtaining the desired frequency response. Basically, the response at any one frequency depends on the active number of electrodes at that frequency. Fowle [24] has developed a synthesis procedure for designing waveforms of this type which works well if large dispersion is used ($T\Delta f > 100$). High-performance waveforms with smaller time–bandwidth products have been designed by using iterative optimization techniques similar to those given in [25]. Both arrays can be weighted by phase weighting because uniform overlap is used. This type of weighting is also useful for increasing the input admittance of a filter, which can be important for reducing insertion losses due to parasitic effects.

B. Distortion Effects

Numerous effects exist which can distort surface-wave interdigital transducer performance such that the impulse-response model is not accurate. The most serious of these effects are; beam spreading and related diffraction effects [26], acoustic reflections at the electrode edges [14], and reflected acoustic signals due to regeneration of acoustic waves [4] by the voltage which is generated on the electrodes of a receiving transducer. Fortunately, beam spreading can be minimized by choosing a sufficiently large electrode overlap width W [see Fig. 1(a)]. Reflections at electrode edges can also be minimized by using the "split-electrode" configuration [27] in which each electrode in a normal interdigital transducer is replaced with a pair of electrodes of half the width and with the same polarity. In this configuration reflections from one electrode have the proper phase such that they are canceled by reflections from the adjacent electrodes. Another popular method for reducing electrode edge reflections is to use quartz instead of lithium niobate substrates which have less reflection for a given metal thickness.

The final effect, reflections due to regeneration of acoustic waves, is an inherent property of the biphase transducer which becomes stronger when the device is electrically matched (i.e., under low-loss conditions). The effect can be reduced by mismatching the device with a low impedance which tends to short out the voltage that causes the regenerated signal. For many device applications this is required since only 12 dB of triple-transit suppression is obtained in a perfectly matched filter. If the same filter were mismatched by an additional 3 dB on each port, approximately 33 dB of triple-transit suppression could be obtained theoretically. Triple-transit effects can also be reduced by using the three-transducer configuration or the unidirectional transducer which are discussed in the following section. However, both these techniques cause additional fabrication complexity which is undesirable and sometimes unacceptable.

The impulse model does not include either beam-spreading or electrode edge reflection effects. Regeneration is included in the model which can be verified by deriving the complete Y-matrix based on the impulse model [21]. The inability to model electrode edge reflections is the only major drawback of this model compared to the modified form of the equivalent-circuit model [14]. However, in designing most filters, the effect of electrode reflections must be made negligible to make the design procedure tractible, and thus this disadvantage of the model is less serious than it appears.

C. Insertion Loss

The sources of insertion loss in surface-wave devices are 1) bidirectionality loss, 2) electrical mismatch loss, 3) parasitic resistance in the transducer pattern, 4) losses in the matching networks, 5) propagation losses in the substrate, 6) losses due to beam spreading, and 7) apodization losses. As discussed below, the first two are the dominant losses for most filters of interest. The remaining ones are usually small if proper care is exercised in design and fabrication.

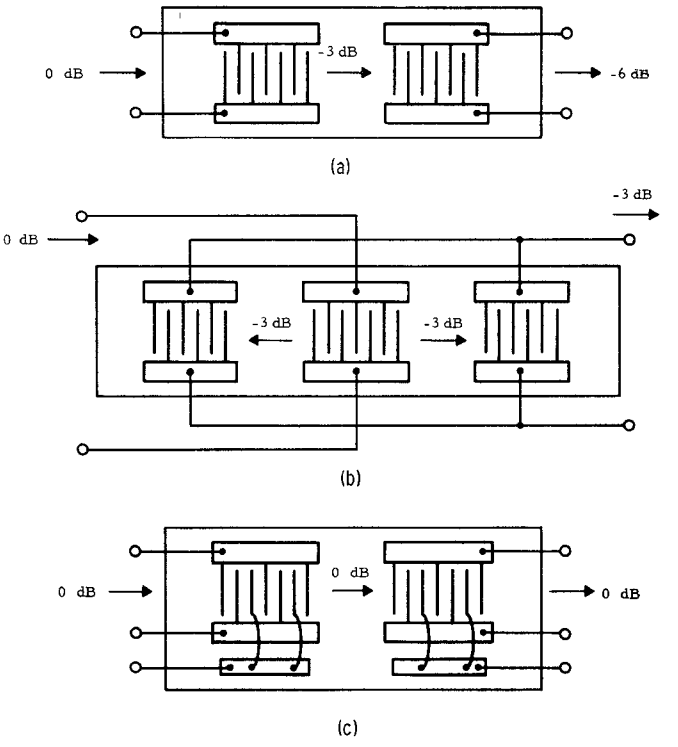

Fig. 12. Three-transducer geometries with varying insertion loss. (a) Two-transducer filter. (b) Three-transducer filter. (c) Unidirectional transducer filter.

The filter configuration shown in Fig. 12(a) has a bidirectionality [4], [28] loss of 6 dB, half of which occurs because the input transducer radiates only half of the power toward the output transducer. The remaining 3 dB occurs at the output transducer, because by reciprocity it can only reconvert half of the acoustic power incident on it into electrical output. Under perfect electrical matching condition, the other half of the power is reradiated as regenerated acoustic waves giving rise to the triple-transit reflections discussed in the preceding section.

Half this bidirectionality loss can be removed by placing a second output transducer on the substrate on the opposite side of the input transducer. The resulting three-transducer configuration shown in Fig. 12(b) has a basic 3-dB loss due to bidirectionality. This configuration also has inherent triple-transit suppression if the center transducer is properly matched, as discussed by Lewis [29]. Unfortunately, this three-transducer configuration cannot be used for dispersive transducers, which limits its usefulness.

It is possible to eliminate the bidirectionality loss completely by using multiphase unidirectional transducers [30], as shown in Fig. 12(c). The multiphase drive removes the bidirectional symmetry and permits complete conversion from electrical signals to acoustic signals traveling in one direction. Thus this structure has no inherent bidirectionality losses. This structure also suppresses triple-transit effects because the output transducer can absorb all the incident acoustic power. The limitations on this transducer are due to added fabrication complexity of the multilayer electrode geometry.

Electrical mismatch is often another major source of loss

TABLE I
SURFACE-WAVE CHARACTERISTICS OF VARIOUS SUBSTRATES

Material	Cut	Propagation Direction	Coupling Coefficient[a] k^2 (%)	Temperature Coefficient (ppm/°C)	Velocity[b] ($\times 10^{-5}$ cm/s)	Capacitance/Pair[c] C_s (pF/cm)
Quartz (*HC*)	−20° rotated *Y*	*X*	0.25	−32	3.209	0.55
Quartz (*ST*)	+42.75° rotated *Y*	*X*	0.16	0	3.157	0.55
$LiNbO_3$	*Y*	*Z*	4.5	−90	3.488	4.6
$Bi_{12}GeO_{20}$	110	001	0.85	−140	1.62	

[a] M. B. Schulz and J. H. Matsinger, "Rayleigh-wave electromechanical coupling constants," *Appl. Phys. Lett.*, vol. 20:9, pp. 367–369, May 1, 1972.
[b] Velocity for a completely free surface.
[c] Reference [11].

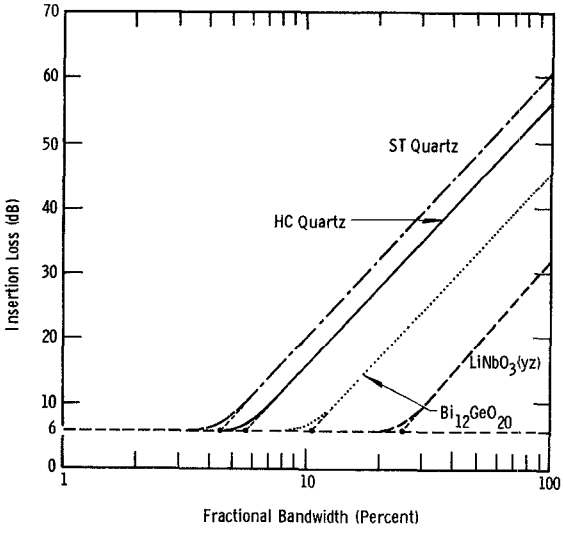

Fig. 13. Minimum achievable insertion loss for two transducers on various substrates.

for two reasons. First, filters are often mismatched as described above to minimize triple transit due to regeneration. Second, transducers are sometimes mismatched to lower the electrical Q of the input so that the matching network does not introduce unwanted bandnarrowing.

The minimum insertion loss which can be achieved at a given fraction bandwidth can be calculated by using the approximate expression for the electrical Q of a transducer given earlier in (29). As long as the Q is less than the reciprocal of the fractional bandwidth, one can easily match the device across the entire bandwidth:

$$Q \leq f_0/\Delta f. \tag{31}$$

If (29) is used in the above expression, one obtains the following restriction on the fractional bandwidth:

$$\frac{\Delta f}{f_0} \leq \sqrt{\frac{4k^2}{\pi}}. \tag{32}$$

If the fractional bandwidth of the transducer is greater than that allowed by (32), it will be assumed that external resistance is used to load the device, thus lowering the Q until (31) is satisfied. If the electrical ports are now matched to this loaded impedance, it can be shown that the additional loss increases at a rate of 12 dB/octave of fractional bandwidth for a two-transducer filter. Fig. 13 shows this minimum insertion loss as a function of fractional bandwidth for several substrates of interest. In this figure *ST*-cut quartz indicates the zero temperature-coefficient cut [31], *HC*-cut quartz is the authors' designation for the highest coupling-coefficient cut available on quartz [32] (−20° rotated *Y*-cut, *X* propagation), the lithium niobate curve is for *Y*-cut, *Z* propagation, and the bismuth germanium oxide is for the 110-cut, 001 propagation. The 6-dB minimum loss which is indicated accounts for bidirectionality. Use of the three-transducer configuration or the unidirectional transducers would uniformly reduce the curves by 3 and 6 dB, respectively. Equation (32) and the use of external resistance, which were assumed in the derivation of Fig. 13, are overly restrictive conditions, and thus theoretically one can achieve lower loss than indicated in the large bandwidth limit, as discussed in [33]. In practice, these curves provide a good estimate of loss expected for typical bandpass filter designs, although some error must be expected for filters with bandwidth over 30 percent due to the uncertainties created by parasitic elements. For moderate bandwidth filters, parasitic elements and propagation losses are normally negligible below 100 MHz. Finally, losses due to beam spreading [26] and apodization [34] typically never exceed 2 dB for most devices.

D. Substrate Choice

Various types and orientations of substrate materials have been demonstrated in laboratory environments [35], but currently the choice is limited to quartz and lithium niobate due to practical considerations, such as cost, ease of fabrication, polishing, temperature stability, reproducibility, reliability, and performance. $Bi_{12}GeO_{20}$ (bismuth germanium oxide) [36] is receiving some use because of its low velocity, but temperature sensitivity and fabrication difficulties limit its acceptance.

Table I summarizes some of the pertinent properties of various substrates of interest. In many applications the temperature coefficient is of primary importance which then dictates that *ST*-cut quartz will be used. This can, however, lead to much increased insertion loss, as was indicated by Fig. 13. It might appear from this figure that lithium niobate is the optimum material for most devices, but, unfortunately, other considerations limit its usefulness. For example, the temperature sensitivity of lithium niobate [19] is high (90 ppm/°C), whereas a range of temperature sensitivities [31] from 0 to 35 ppm/°C are available on quartz. Also, the higher coupling lithium niobate is affected more severely by various distortion effects, such as reflection and regeneration [4], especially for the devices with fractional bandwidths below 10 percent. Thus the lower coupling coefficient of quartz can actually be an advantage for these narrower fractional bandwidth devices.

Other parameters which may be important in choice of a substrate include the velocity of propagation, beam-spreading and beam-steering effects [26], and the required tolerances on substrate orientation [37]. Low-velocity materials minimize the overall device size for filters with a large amount of

time delay, whereas high velocities are useful for reducing the resolution requirements for fabrication of high-frequency devices (>1 GHz). For devices with large time delays, the beam-spreading and beam-steering effects are also important considerations because certain materials tend to maintain a well-collimated surface-wave beam over much larger distances than other materials. For example, quartz generally tends to spread the acoustic beam faster than one would find based on an isotropic diffraction theory, while *Y*-cut *Z*-propagating lithium niobate is partially selfcollimating.

V. Design Summary

The primary contributions of this paper to designing surface-wave filters are, 1) a simple method for predicting transducer input impedance which allows various design tradeoffs to be made, and 2) methods for obtaining desirable impulse responses. The application of this information is shown in this section by giving a brief summary of a design procedure used by the authors which allows one to make design decisions in an order which builds on preceding decisions. The procedure can be summarized as follows.

1) Divide the desired filter response into two transducer responses to be realized as input and output transducers, as discussed in Section IV-A.

2) Choose a substrate based on insertion loss, temperature, and other characteristics, as outlined in Section IV-D.

3) Determine the minimum required impulse-response length for each transducer, and hence determine the required device length. Fig. 3 provides the required information for bandpass filters.

4) The information on minimum device length can be used to determine the minimum beamwidth required to prevent beam spreading, as outlined in [26].

5) Evaluate the approximate input and output admittances for this minimum-size device by using Fig. 9. If they are too small, one can increase the beamwidth or add dispersion to the filter responses. If they are too large, series connection techniques can be used to lower the admittance. Parasitic resistance and parasitic capacitance are important in this tradeoff. The general features of the filter design are now known even though the exact electrode placements have not been determined.

6) Triple-transit and electrode edge distortion are now determined for the transducers with the desired bandwidth, beamwidth, dispersion, and approximate source and load admittances. The modified equivalent-circuit or impulse-response model is used, depending on whether it is necessary to evaluate edge reflections. If triple transit or distortion are unacceptably large, the design is modified, as discussed in Section IV-B, until an acceptably low distortion is predicted.

7) The filter package is designed so that parasitics associated with it can be estimated and be included along with other parasitic effects in a comprehensive equivalent circuit for the packaged device. Matching networks are designed for these circuits and the transfer function for each transducer, including electrical effects, is calculated resulting in an expression similar to (30). The acoustic admittances in this expression can be approximated using (12)–(14) or (19). Each unmatched transducer response can now be modified to compensate for the electrical loading effect.

8) An impulse response for realizing the modified transducer response is determined using techniques discussed in Section II-B and Appendix I.

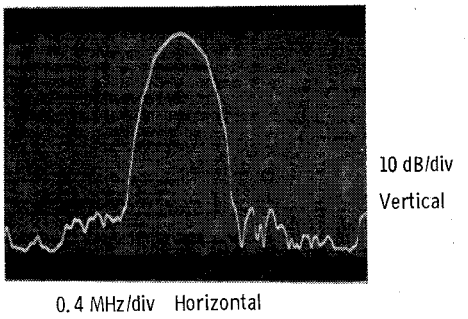

Fig. 14. Response of PRC-95 Transponder IF filter; center frequency—10.7 MHz; bandwidth—0.38 MHz.

The importance of the impulse model is clearly demonstrated by the procedure because steps 2) and 5)–7) all benefit significantly from the model. This procedure allows one to make design tradeoffs in a straightforward manner, such that a high-performance device is obtained at an acceptible design cost.

VI. Filter Examples

Three representative surface-wave filters will be discussed to illustrate that good performance can be obtained by making the design tradeoffs described in the previous sections.

A. PRC-95-Field Survival Radio

The AN/PRC-95/DME Transponder is a prototype *L*-band 20-W transponder which was developed for locating downed fliers. The major system problem was that the receiver had to respond instantaneously over an 85-dB range of signal levels with constant time delay and without degradation of the pulse performance. Conventional automatic gain-control techniques were not adequate. Instead, a system of progressive limiting amplifiers was developed with sufficient bandwidth to eliminate time-delay variations over a wide dynamic range. A compact linear-phase bandpass filter was required in the IF stage with bandpass and time delay that were unaffected by the changing impedance due to the limiting of the stages around the filter. The filter selectivity was required to provide 50-dB rejection for pulses at ± 1 MHz of the center frequency.

A surface-wave bandpass filter was designed which had a modified Gaussian bandpass characteristic, as shown in Fig. 14. This response was chosen for minimum pulse distortion with maximum out-of-band rejection. The device was built on a $0.75 \times 0.3 \times 0.08$-in quartz substrate with a center frequency of 10.7 MHz. Midband insertion loss was 18 dB with a 3-dB bandwidth of 0.4 MHz and a 40-dB bandwidth of 1.0 MHz. The phase response was linear over the entire 40-dB bandwidth, which resulted in extremely good pulse fidelity. The sidelobes on the high-frequency side of the response are due to bulk shear modes in the quartz propagating medium. The filter was mounted directly on a thick-film hybrid substrate and matched electrically by using subminiature tuneable *H*-core inductors resulting in a high-performance compact IF module.

B. 300-MHz Front-End Filter

Fig. 15(a) shows the frequency response of a 300-MHz 2.5-MHz bandwidth filter which has been electrically matched to achieve a minimum midband loss of 6 dB. This response was achieved by using a three-transducer configuration, as was

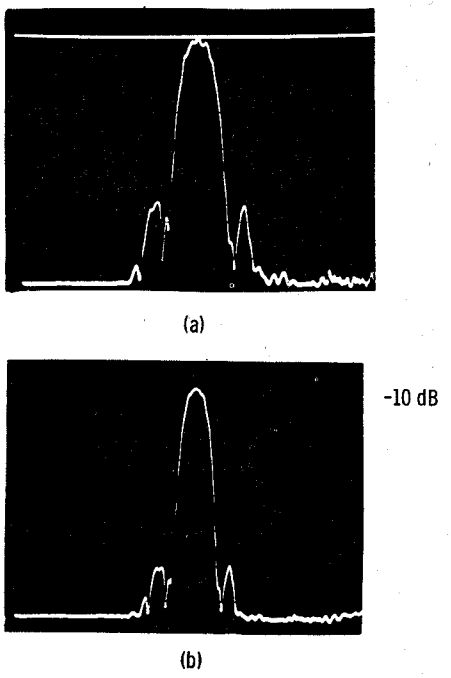

Fig. 15. 300-MHz bandpass filter. (a) Matched for minimum insertion loss. $f_0 = 300$ MHz; REF $= -6$ dB; vertical scale equals 10 dB/div; horizontal scale equals 2.5 MHz/div. (b) $f_0 = 300$ MHz; REF $= -10$ dB; vertical scale equals 10 dB/div; horizontal scale equals 3 MHz/div.

shown in Fig. 12. The center transducer was apodized for sidelobe rejection and two outer arrays were unweighted. The 6-dB loss consists of 3-dB bidirectionality loss, 1.2 dB due to the apodization of the center transducer and 1.8 dB due to parasitic losses. A 60-MHz scaled version of this same filter had a minimum matched loss less than 5 dB. The filters were built on ST-quartz substrate which measured $0.3 \times 0.12 \times 0.02$ in. The ripple which is seen on the frequency response is due to triple-transit effects. The triple-transit suppression of the three-transducer configuration [29] is spoiled by the apodization of the center array.

Fig. 15(b) shows the response of the same filter when it is mismatched to yield 10-dB loss. Two interesting differences exist between the two cases. First, a significant improvement is observed in the bandpass ripple which corresponds to a reduction of the triple-transit effect, as discussed earlier in Section IV-B. Second, almost 5-dB improvement in sidelobe rejection is obtained. This is an example of the sidelobe degradation effect due to electrical loading which was discussed earlier in Section III-G.

Note that in both cases ultimate rejection in excess of 60 dB is obtained. Also, by proper electrical design of the filter package, direct electrical crosstalk has been suppressed in excess of 70 dB in spite of the extremely small filter size.

C. Low Shape Factor Filter

Fig. 16(a) shows the frequency response for a 7-percent fractional bandwidth amplifier module [38] which uses a surface-wave filter for bandpass shaping. The filter response is centered at 168 MHz with a 12-MHz 3-dB bandwidth and a 13.5-MHz 40-dB bandwidth. The filter above has a 14-dB midband insertion loss, while the single stage amplifier integrated into the same package exhibits a gain of 20 dB. The skirt selectivity exceeds 80 dB/MHz for the first 25 dB. This response was obtained by using a combination of amplitude

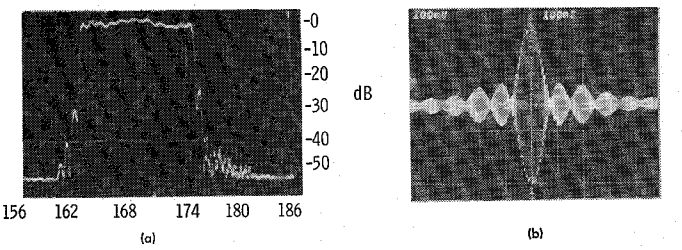

Fig. 16. Low shape factor VHF bandpass filter. (a) Frequency response: 12-MHz (7-percent) bandwidth; 14-dB insertion loss. (b) Sin x/x impulse response indicates linear phase and rectangular bandpass.

and phase weighting and was designed by iterative optimization techniques. Opposite dispersion was used in the input and output transducers so that the overall response was nondispersive. The near ideal sin X/X impulse response of the device shown in Fig. 16(b) corresponds to the linear phase and rectangular bandpass characteristics.

A major reason for using dispersive transducers was to reduce insertion loss due to parasitic resistance and capacitance. The minimum size design [see Section V, step 5)] had an input impedance of 18 kΩ in parallel with 1.5 pF. Parasitic package capacitance would have more than doubled the susceptance, thereby aggravating an already severe matching problem. By using approximately 12:1 dispersion in each transducer, and increasing the beamwidth, the input impedance was lowered to 1.5 kΩ in parallel with 20 pF.

VII. Conclusions

Interdigital surface-wave filters have been demonstrated to be a practical technology with many advantages for VHF and UHF filters such as; 1) flexibility for realizing a wide range of filter characteristics, 2) small size, 3) low cost as a result of easy fabrication, 4) reproducibility, 5) wide dynamic range and, in certain cases, 6) low loss, and 7) excellent temperature stability. The range of achievable performance parameters includes: 1) center frequencies from 10 MHz to 1 GHz, 2) bandwidths from 50 kHz to 80 percent of the center frequency, 3) frequency sidelobe rejection in excess of 50 dB for bandpass filters, 4) time sidelobe rejection in excess of 30 dB for pulse-compression filters, 5) pulse-compression ratios up to 1000:1, and 6) insertion losses as low as 6 dB for certain filters. Further discussion on the range of achievable performance is given by other papers in this issue [15], [17].

The central point of this paper has been the development of an impulse-response model and its application to device design. The features of this model are that accurate predictions of device performance can be made with considerably less computation effort than required with the equivalent-circuit model [4].

The simplicity of this technique makes it much more useful for filter design than previous models. Specifically, 1) the universal impedance curves (Fig. 9) are valuable for making design tradeoffs without requiring a complete device reanalysis each time a parameter is changed; 2) the expression for radiation Q [see (29)] allowed the development of minimum achievable insertion-loss curves for various substrates as a function of fractional bandwidth; and 3) the effect of electrical loading can be accurately calculated such that a filter design can be compensated for it. As a result, a rational design procedure has been developed, as described in Section V, through which high-performance filters may be synthesized with minimum effort and expense.

Appendix I
Optimum Impulse Responses for Bandpass Functions

The finite length of surface filters means that the impulse responses which can be realized by surface-wave filters must also be of finite duration. As explained earlier in conjunction with Fig. 2, the optimization problem is to determine the impulse response with the shortest length which will satisfy a given frequency specification. This problem has received considerable attention in the literature for designing nonrecursive digital filters. Application of digital-filter design procedures requires that an appropriate translation be made from the sampled waveforms used in digital filters to the continuous waveforms characteristic of surface-wave impulse responses.

This appendix summarizes a "window-function" technique described by Helms [9] which produces good (and sometimes even the best possible) skirt selectivity and sidelobe rejection. The achieved frequency response is the convolution of the desired response with a Dolph–Chebyshev function $D(\omega)$ whose principal lobe has a width that is as small as possible for a given sidelobe level and impulse-response length. The inverse Fourier transform of $D(\omega)$ is a finite time-duration function $d(t)$.

To use the window-function technique, one calculates the inverse Fourier transform of the desired frequency response which is normally of infinite time extent. This function is then multiplied by the appropriate window function $d(t)$ which has the effect of weighting the function and smoothly truncating it to a finite length. The resulting frequency spectrum can be evaluated for suitability by taking the Fourier transform of the truncated time function.

The Dolph–Chebyshev function is given by

$$\frac{\cos\left[P\cos^{-1}\left(Z_0\cos\pi f\right)\right]}{\cosh\left[P\cosh^{-1}\left(Z_0\right)\right]}$$

where parameters P and Z_0 are chosen to make the achieved frequency response fulfill the requirements for selectivity and ripple. The value of P determined by this procedure is as small as possible since the Dolph–Chebyshev function shown above has the smallest sidelobe level for a given main-lobe width, and, conversely, the smallest main-lobe width for a given sidelobe level. A more detailed description of this procedure is contained in [9].

Based on this technique, one can write an approximate relationship for the minimum time length required to achieve a specified sidelobe level R_2 and a specified transition bandwidth B_1 in a bandpass filter impulse response:

$$\tau_{\min} \simeq (0.73/B_1)\log R_2.$$

This is only an approximate relationship and, further, the above technique is not exactly optimum for bandpass responses. It is close enough, however, to be adequate for most filter designs. Iterative procedures are available [25] for obtaining a true optimum response but these are generally very complex to use.

Appendix II
Instantaneous Frequency Dependence of the Impulse Response

Construction of an impulse response for a given device geometry requires knowledge of the effect of finger separation (i.e., instantaneous frequency) on the magnitude of the generated acoustic response. The basis of the determination is a scaling law [10] which applies to any device which can be described by the linear elastic equations of motion coupled to Maxwell's electromagnetic equations of motion by the piezoelectric effect. If all the dimensions of a device are uniformly reduced in size by a factor α, then all the properties of the device (as described by the appropriate variables) will remain unchanged except for a corresponding scale change of the time dependence. An appropriate set of variables are the electric field $\boldsymbol{E}$, the magnetic field $\boldsymbol{H}$, the acoustic velocity $\dot{\boldsymbol{u}}$, and the acoustic stress $\boldsymbol{T}$, which may then be related to the device terminal voltage and current. Electrical and acoustic losses must be omitted for scaling to hold.

It will now be shown from the scaling law and conservation of energy that the amplitude response varies as $f_t^{3/2}$. Consider two similar transducers with equal beamwidths and with an equal number of electrodes, but one has a smaller electrode spacing and thus a higher center frequency. One can show by means of the scaling law that the input admittance of the higher frequency transducer is equal to the input admittance of the lower frequency transducer scaled to the higher frequency and multiplied by the scaling factor α:

$$Y_s(\omega) = \alpha Y_0\left(\frac{\omega}{\alpha}\right). \tag{33}$$

The impulse responses will also be similar except for an amplitude factor to be determined from conservation of energy:

$$h_s(t) = \beta h_0(\alpha t). \tag{34}$$

The variable h is proportional to the square root of the acoustic power as discussed in Section III-A.

The energy in both impulse responses of (34) is determined by integrating over their time duration (equal number of cycles in each case). Then,

$$\frac{E_s}{E_0} = \frac{\beta^2}{\alpha}. \tag{35}$$

The energy absorbed from the δ-function impulse by the input admittance is determined by performing a similar integral in the frequency domain:

$$\frac{E_s}{E_0} = \alpha^2. \tag{36}$$

Solving (35) and (36) for β, we find that

$$\beta = \alpha^{3/2}. \tag{37}$$

Thus two transducers which have identical beamwidths but different center frequencies will have impulse responses whose amplitude ratio is directly proportional to the ratio of the center frequencies to the three halves power.

Acknowledgment

The authors wish to thank L. T. Claiborne and H. G. Vollers for their contributions toward developing the techniques and filters described here. In addition, they wish to thank T. M. Reeder for making numerous valuable suggestions during preparation of the manuscript.

References

[1] R. M. White, "Surface elastic-wave propagation and amplification," *IEEE Trans. Electron Devices*, vol. ED-14, pp. 181–189, Apr. 1967.
[2] R. H. Tancrell and M. G. Holland, "Acoustic surface wave filters," *Proc. IEEE*, vol. 59, pp. 393-409, Mar. 1971.

[3] C. C. Tseng, "Frequency response of an interdigital transducer for excitation of surface elastic waves," *IEEE Trans. Electron Devices*, vol. ED-15, pp. 586–594, Aug. 1968.
[4] W. R. Smith *et al.*, "Analysis of interdigital surface wave transducers by use of an equivalent circuit model," *IEEE Trans. Microwave Theory Tech. (Special Issue on Microwave Acoustics)*, vol. MTT-17, pp. 856–864, Nov. 1969.
[5] W. T. Cochran *et al.*, "What is the fast Fourier transform?", *Proc. IEEE*, vol. 55, pp. 1664–1674, Oct. 1967.
[6] W. P. Mason, Ed., *Physical Acoustics*. New York: Academic Press, 1964. (This series of volumes contains many review articles on bulk wave phenomena and devices.)
[7] E. A. Guillemin, *Theory of Linear Physical Systems*. New York: Wiley, ch. 16, 1963.
[8] F. F. Kuo and J. F. Kaiser, Eds., *Systems Analysis by Digital Computer*. New York: Wiley, ch. 7, 1966.
[9] H. D. Helms, "Nonrecursive digital filters: Design methods for achieving specifications on frequency response," *IEEE Trans. Audio Electroacoust. (Special Issue on Digital Filters: The Promise of LSI Applied to Signal Processing)*, vol. AU-16, pp. 336–342, Sept. 1968.
[10] W. S. Jones, C. S. Hartmann, and L. T. Claiborne, "Surface wave devices," Office of Naval Research, Final Rep. N00014-69-C-0173 [NR017-503/10-23-69(421)], Apr. 1971.
[11] H. Engan, "Excitation of elastic surface waves by spatial harmonics of interdigital transducers," *IEEE Trans. Electron Devices*, vol. ED-16, pp. 1014–1017, Dec. 1969.
[12] A. L. Nalamwar and M. Epstein, "Immittance characterization of acoustic surface wave transducers," *Proc. IEEE* (Lett.), vol. 60, pp. 336–337, Mar. 1972.
[13] R. M. Bracewell, *The Fourier Transform and Its Applications*. New York: McGraw-Hill, 1965.
[14] W. S. Jones, C. S. Hartmann, and T. D. Sturdivant, "Second order effects in surface wave devices," *IEEE Trans. Sonics Ultrason.*, vol. SU-19, pp. 368–377, July 1972.
[15] H. M. Gerard, W. R. Smith, W. R. Jones, and J. B. Herrington, "The design and applications of highly dispersive acoustic surface-wave filters," this issue, pp. 176–186.
[16] W. S. Jones, R. A. Kempf, and C. S. Hartmann, "Practical surface wave chirp filters for modern radar systems," *Microwave J.*, vol. 15, no. 5, pp. 43–80, May 1972.
[17] D. T. Bell, Jr., J. D. Holmes, and R. V. Ridings, "Application of acoustic surface-wave technology to spread spectrum communications," this issue, pp. 263–271.
[18] P. M. Grant, J. H. Collins, B. J. Darby, and D. P. Morgan, "Potential applications of acoustic matched filters to air-traffic control systems," this issue, pp. 288–300.
[19] W. S. Jones, C. S. Hartmann, and L. T. Claiborne, "Evaluation of digitally coded acoustic surface-wave matched filters," *IEEE Trans. Sonics Ultrason.*, vol. SU-18, pp. 21–27, Jan. 1971.
[20] C. S. Hartmann, "An impulse response model predicting SWD input admittance," presented at the Ultrasonics Symp., Miami Beach, Fla., Dec. 1971. Abstract published *IEEE Trans. Sonics Ultrason.*, vol. SU-19, pp. 399–400, July 1972.
[21] R. F. Mitchell and N. H. C. Reilly, "Equivalence of δ-function and equivalent-circuit models for interdigital acoustic-surface-wave transducers," *Electron. Lett.*, vol. 8, pp. 329–331, June 29, 1972.
[22] W. R. Smith, H. M. Gerard, and W. R. Jones, "Analysis and design of dispersive interdigital surface-wave transducers," *IEEE Trans. Microwave Theory Tech.*, vol. MTT-20, pp. 458–471, July 1972.
[23] F. G. Marshall, C. O. Newton, and E. G. S. Paige, "Theory and design of the surface acoustic wave multistrip coupler," and "Surface acoustic wave multistrip components and their applications," this issue, pp. 206–215 and 216–225.
[24] E. N. Fowle, "The design of FM pulse compression signals," *IEEE Trans. Inform. Theory*, vol. IT-10, pp. 61–67, Jan. 1964.
[25] R. W. Hankins, *Design Procedure for Equiripple Nonrecursive Digital Filters*, Mass. Inst. Technol., Res. Lab. of Elec., Tech. Rep. 485, May 12, 1972.
[26] T. L. Szabo and A. J. Slobodnik, Jr., "The effect of diffraction on the design of acoustic surface wave devices," *IEEE Trans. Sonics Ultrason.*, to be published.
[27] T. W. Bristol, W. R. Jones, P. B. Snow, and W. R. Smith, "Applications of double electrodes in acoustic surface wave device design," in *1972 IEEE Ultrasonics Symp. Proc.*, pp. 343–345, Oct. 4–7, 1972.
[28] W. R. Smith *et al.*, "Design of surface wave delay lines with interdigital transducers," *IEEE Trans. Microwave Theory Tech. (Special Issue on Microwave Acoustics)*, vol. MTT-17, pp. 865–873, Nov. 1969.
[29] M. F. Lewis, "Triple-transit suppression in surface-acoustic-wave devices," *Electron. Lett.*, vol. 8, pp. 553–554, Nov. 16, 1972.
[30] C. S. Hartmann, W. S. Jones, and H. Vollers, "Wideband unidirectional interdigital surface wave transducers," *IEEE Trans. Sonics Ultrason.*, vol. SU-19, pp. 378–381, July 1972.
[31] M. B. Schulz and M. G. Holland, "Surface acoustic wave delay lines with small temperature coefficient," *Proc. IEEE* (Lett.), vol. 58, pp. 1361–1362, Sept. 1970.
[32] G. A. Coquin and H. F. Tiersten, "Analysis of the excitation and detection of piezoelectric surface waves in quartz by means of surface electrodes," *J. Acoust. Soc. Amer.*, vol. 41, pt. 2, pp. 921–939, Apr. 1967.
[33] T. M. Reeder and W. R. Sperry, "Broad-band coupling to high-Q resonant loads," *IEEE Trans. Microwave Theory Tech.*, vol. MTT-20, pp. 453–458, July 1972.
[34] R. A. Waldron, "Power transfer factors for nonuniformly irradiated interdigital piezoelectric transducers," *IEEE Trans. Sonics Ultrason.*, vol. SU-19, pp. 448–453, Oct. 1972.
[35] A. J. Slobodnik, Jr., and E. D. Conway, *Microwave Acoustics Handbook*, AFCRL Rep. AFCRL-70-0164, PSRP 414, Mar. 1970.
[36] J. H. Collins, P. J. Hagon, and G. R. Pulliam, "Evaluation of new single crystal piezoelectric materials for surface wave applications," *Ultrason.*, vol. 8, pp. 218–226, Oct. 1970.
[37] D. T. Bell, "Phase errors in long surface wave devices," in *1972 IEEE Ultrasonics Symp. Proc.*, pp. 420–423, Oct. 4–7, 1972.
[38] T. F. Cheek, R. M. Hays, and C. S. Hartmann, "A wide-band low-shape-factor amplifier module using an acoustic surface-wave bandpass filter," *IEEE J. Solid-State Circuits*, vol. SC-8, pp. 66–70, Feb. 1973.